Impact of Species-Dependent Differences on Screening, Design, and Development of MAO B Inhibitors

Laura Novaroli,[†] Antoine Daina,[†,‡] Elisabeth Favre,[†] Juan Bravo,[†] Angelo Carotti,[§] Francesco Leonetti,[§] Marco Catto,[§] Pierre-Alain Carrupt,[†] and Marianne Reist*[,†]

LCT- Pharmacochemistry, School of pharmaceutical sciences, University of Geneva, University of Lausanne, Suisse, 30 Quai Ernest Ansermet, CH-1211 Geneva 4, Switzerland, and Dipartimento Farmaco-Chimico, University of Bari, I-70125 Bari, Italy

Received April 13, 2006

The impact of species-dependent differences between human and rat MAO B on inhibitor screening was evidenced for two classes of compounds, coumarin and 5*H*-indeno[1,2-*c*]pyridazin-5-one derivatives. All examined compounds have shown a greater inhibitor potency toward human MAO B than toward rat MAO B. Moreover, no correlation was found between human and rat pIC_{50} values. These divergences have important implications for the design and development of drugs involved in the MAO B metabolic pathway, suggesting that results obtained using rat enzyme cannot be extrapolated to human CNS, a priori. Indeed, the selection of a hit compound for lead generation could be different using human rather than rat enzyme. Moreover, the influence of substituents on the in vitro inhibition of human MAO B was markedly different between homogeneous series of coumarin and 5*H*-indeno[1,2-*c*]pyridazin-5-one derivatives, suggesting different binding modes, a hypothesis clearly supported by molecular docking simulations of inhibitors into the active site of human MAO B.

Introduction

Interest in selective inhibitors of monoamine oxidase B (MAO B,[a] EC 1.4.3.4) has increased in the last years due to their therapeutic potential in aging related neurodegenerative diseases such as Alzheimer's disease (AD) and Parkinson's disease (PD).[1,2] Indeed, studies involving activity measurements of the two MAO isoforms, MAO A and MAO B, in postmortem brain have shown an age-related increase in MAO B but a constant activity of the isoenzyme A. Moreover, ontogenetic studies have demonstrated that MAO B activity stays unchanged until the 60th year of life and then increases nonlinearly.[3,4] Because MAO B is predominantly located in glial cells,[5,6] the increase of this enzyme with age may be attributed to glial cell proliferation associated with neuronal loss.[5,6] An age-related increase of brain MAO B activity is believed to cause an augmentation in oxidative stress.[7] Indeed, hydrogen peroxide (H_2O_2) produced during amine oxidation may interact with free iron to form highly reactive hydroxyl radicals that can damage nucleic acids, proteins, and membrane lipids, leading to neuronal degeneration.[2] Thus, MAO B inhibitors, which decrease the rate of MAO B-catalyzed oxidative deamination and, consequently, the production of reactive oxygen species (ROS), might beneficially contribute to the treatment of Alzheimer's and Parkinson's diseases via neuroprotection.[8]

Moreover, in the context of Parkinson's disease, MAO B inhibitors present a second therapeutic application due to the fact that MAO is one of dopamine's major metabolizing enzymes. As MAO B is present in excess in the tissue in which metabolization occurs, the inhibition of the isoenzyme B blocks the metabolism of dopamine, enhancing both the endogenous dopamine level and dopamine produced from exogenously administered precursor levodopa (L-DOPA).[1,9] Indeed, the inhibition of dopamine degradation by MAO B inhibitors combined with supplementation of dopamine by L-DOPA has been shown to be successful in the treatment of PD patients.[10]

In the literature, brain,[11] liver,[12] and, especially, blood platelets[13] have been widely described as human MAO B sources to screen inhibitors. Above all, blood platelets, containing prevalently the B form of monoamine oxidase, have provided a clinically useful source for selective studies of the properties of this isoform.[14] However, for ethical and practical reasons, human tissues are difficult to obtain. In contrast, animal tissues, such as rat brain[15−18] or rat liver,[19,20] are easily accessible sources for in vitro screening of MAO B inhibitors, and therefore, rodents have been employed for most in vitro studies.

Nevertheless, species-dependent differences in substrate specificity and inhibitor selectivity have been reported by several authors. For example, important differences in the interaction of the anticonvulsant milacemide and some analogues with human and rat MAO B have been described by O'Brien et al.[21] Moreover, human brain and human platelet MAO B have been shown to differ from rat brain enzyme in sensitivity to inhibition by some tricyclic antidepressant drugs. These antidepressant drugs inhibited rat brain MAO B to a greater extent than either human platelet or brain MAO B.[22] These differences between species have been supported by immunological data that show that a monoclonal antibody, raised toward human platelet MAO B, binds to human brain MAO B but does not bind to the rat or mouse enzyme.[23,24] Recently, Geha et al. have reported that despite the high homology between rat and human MAO B (88% sequence identity, 93% sequence homology), differences in the secondary and tertiary structures may exist and influence the substrate specificity and inhibitor sensitivity in the two species.[25] These divergences reported by several authors have important implications for comparative studies of drugs involved in the MAO B metabolic pathway, suggesting that results

* Corresponding author. E-mail: marianne.reistoechslin@pharm.unige.ch. Tel.: +41 22 379 33 65. Fax: +41 22 379 33 60.
† University of Geneva, University of Lausanne.
‡ Present address: Syngenta Crop Protection AG, P.O. Box, CH-4002 Basel, Switzerland.
§ University of Bari.

[a] Abbreviations: AD, Alzheimer's disease; BFGS, minimization method of Broyden, Fletcher, Goldfarb, and Shanno; MAO A, monoamine oxidase A; MAO B, monoamine oxidase B; MLP, molecular lipophilicity potential; PD, Parkinson's disease; PDB, protein data bank; ROS, reactive oxygen species.

10.1021/jm060441e CCC: $33.50
Published on Web 09/26/2006

Table 1. Supersomes and Rat Brain MAO B Inhibitory Activities of Coumarin Derivatives (Series I)

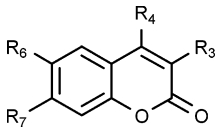

cmpd	R3	R4	R6	R7	pIC_{50} Supersomes[a]	pIC_{50} rat[a]	ΔpIC_{50}[b,c]
C-2	H	H	H	$OCH_2C_6H_5$	8.77 ± 0.04	7.26 ± 0.02	1.51
C-3	H	H	H	$CH_2OC_6H_5$	7.19 ± 0.02	7.07 ± 0.04	0.12
C-4	H	H	H	$CH_2NHC_6H_5$	7.24 ± 0.06	5.67 ± 0.02	1.57
C-10	H	CH_3	H	$OCH_2C_6H_5$	8.80 ± 0.06	7.74 ± 0.03	1.06
C-11	H	CH_3	H	$OCH_2C_6H_4$-3′-NO_2	8.49 ± 0.09	7.88 ± 0.03	0.61
C-12	H	C_6H_5	H	$OCH_2C_6H_5$	6.59 ± 0.05	5.40	1.19
C-15	CH_3	CH_3	H	$OCH_2C_6H_5$	8.97 ± 0.13	8.36 ± 0.06	0.61
C-16	CH_3	CH_3	H	$NHCH_2C_6H_5$	8.86 ± 0.08	6.79 ± 0.02	2.06
C-19	$(CH_2)_3$		H	$OCH_2C_6H_5$	9.04 ± 0.14	8.46 ± 0.06	0.58
C-20	$(CH_2)_4$		H	$OCH_2C_6H_5$	8.75 ± 0.04	7.87 ± 0.02	0.87
C-21	$(-CH{=}CH)_2$		H	$OCH_2C_6H_5$	8.95 ± 0.09	7.30 ± 0.02	1.64
C-23	CH_3	CH_3	H	$NHCOC_6H_5$	8.06 ± 0.03	6.72 ± 0.03	1.34
C-24	CH_3	CH_3	H	$OSO_2C_6H_5$	7.80 ± 0.11	5.28 ± 0.02	2.51
C-26	CH_3	CH_3	H	$OSO_2C_6H_4$-4-OCH_3	6.70 ± 0.05	4.77 ± 0.01	1.93
C-30	CH_3	CH_3	OH	$OCH_2C_6H_5$	8.41 ± 0.05	7.55 ± 0.03	0.86
C-31	CH_3	CH_3	$OCH_2C_6H_5$	OH	6.90 ± 0.07	5.51 ± 0.03	1.39
C-75	H	H	H	$OSO_2C_6H_5$	5.65 ± 0.06	4.26 ± 0.02	1.39

[a] Standard errors for Supersomes calculated for the sigmoidal regression, not comparable with the standard deviation calculated on the average of different assays for rat enzyme. [b] ΔpIC_{50}: pIC_{50} Supersomes − pIC_{50} rat. [c] Highly significant ($P < 0.0001$, paired two-tailed student's t-test) difference of inhibition potency between human and rat MAO B.

obtained using rat enzyme can be extrapolated to human CNS only with caution.

In an attempt to provide a better understanding of the limitations of the rat model to predict human MAO B activity and inhibitor specificity, two classes of compounds, coumarin ($n = 33$) and 5*H*-indeno[1,2-*c*]pyridazin-5-one derivatives ($n = 29$), known as rat MAO B inhibitors,[26,27] were tested on human MAO B. Human-cloned enzyme obtained from Baculovirus-infected insect cells (Supersomes MAO B, BD Gentest) was used as human MAO B source. The undoubted reliability in using this enzyme source has been reported previously.[28]

Important species-dependent differences in MAO B inhibitor specificity between human and rat were evidenced for both classes of compounds investigated. Indeed, all compounds showed a greater inhibitor potency toward human than toward rat MAO B, and no correlation was found between inhibitor potencies toward the two enzymes. Moreover, marked differences between the two homogeneous series, coumarin series II and 5*H*-indeno[1,2-*c*]pyridazin-5-one series IV, concerning the influence of substituents on the in vitro inhibitory activity of human MAO B were observed. To elucidate these different in vitro inhibition patterns of the two homogeneous series, molecular docking of these series into the active site of human MAO B was performed.

Results and Discussion

Classification of Tested Compounds. To investigate the possible differences between human and rodent enzyme, inhibitor potencies of two different classes of compounds known as rat MAO B inhibitors, coumarin and 5*H*-indeno[1,2-*c*]pyridazin-5-one derivatives, were determined for human MAO B. Rat MAO B inhibition values have been reported by Gnerre et al.[26] for coumarin derivatives and by Kneubühler et al.[27] for 5*H*-indeno[1,2-*c*]pyridazin-5-one derivatives, respectively.

Among the 71 coumarin derivatives published by Gnerre et al.,[26] 33 compounds covering the whole range of inhibitor potencies determined with rat enzyme, were chosen. In addition, coumarin derivative (**C-75**) synthesized later[28] was also tested. To compare the inhibitor selectivity of the two enzyme sources,

Table 2. Supersomes and Rat Brain MAO B Inhibition Data for 7-X-Substituted Benzyloxy-3,4-dimethylcoumarins (Series II)

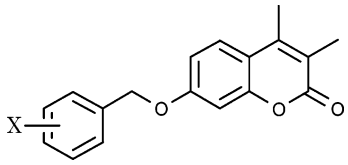

cmpd	X	pIC_{50} Supersomes[a]	pIC_{50} rat[a]	ΔpIC_{50}[b,c]
C-15	H	8.97 ± 0.13	8.36 ± 0.06	0.61
C-50	2-CN	8.71 ± 0.06	7.64 ± 0.03	1.07
C-51	3-CH_3	8.92 ± 0.17	8.36 ± 0.06	0.56
C-53	3-OCH_3	8.78 ± 0.23	8.44 ± 0.04	0.34
C-54	3-OCF_3	8.44 ± 0.07	7.94 ± 0.03	0.51
C-56	3-$NHCOCH_3$	8.10 ± 0.16	6.60 ± 0.03	1.50
C-57	3-F	9.04 ± 0.15	8.55 ± 0.05	0.49
C-58	3-Cl	8.67 ± 0.15	8.48 ± 0.05	0.19
C-59	3-CF_3	8.37 ± 0.11	8.24 ± 0.04	0.13
C-60	3-CN	8.85 ± 0.02	7.97 ± 0.03	0.88
C-61	3-NO_2	8.96 ± 0.07	8.59 ± 0.05	0.37
C-62	4- CH_3	8.86 ± 0.07	8.21 ± 0.03	0.65
C-63	4-F	8.81 ± 0.13	8.52 ± 0.06	0.29
C-64	4-Cl	8.83 ± 0.05	8.59 ± 0.03	0.24
C-65	4-CN	8.63 ± 0.06	8.43 ± 0.05	0.19
C-66	4-NO_2	8.95 ± 0.06	8.07 ± 0.02	0.88
C-71	pentafluoro	8.79 ± 0.07	8.23 ± 0.04	0.56

[a] Standard errors for Supersomes calculated for the sigmoidal regression, not comparable with the standard deviation calculated on the average of different assays for rat enzyme. [b] ΔpIC_{50}: pIC_{50} Supersomes − pIC_{50} rat. [c] Highly significant ($P < 0.0001$, paired two-tailed student's t-test) difference of inhibition potency between human and rat MAO B.

the same classification as given by Gnerre et al.[26] was held, that is, tested compounds were divided into two series: a first series with variations mainly in positions 3, 4, and 7 of the coumarin nucleus (series I, Table 1, $n = 17$) and a second series of 7-benzyloxysubstituted congeners of 3,4-dimethylcoumarin (series II, Table 2, $n = 17$).

The same selection criterion adopted for coumarin derivatives, well-distributed rat MAO B inhibitor potencies, was applied to choose 29 indeno[1,2-*c*]pyridazin-5-one derivatives among the 66 published by Kneubühler et al.[27] Following the classification of the authors,[27] the compounds were divided in two series: a

Table 3. Supersomes and Rat Brain MAO B Inhibition Data for 5*H*-indeno[1,2-*c*]pyridazin-5-one Derivatives (Series III)

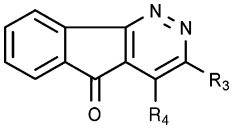

cmpd	R3	R4	pIC$_{50}$ Supersomes[a]	pIC$_{50}$ rat[a]	ΔpIC$_{50}$[b,c]
IP-4	CH_3	H	5.56 ± 0.21	4.13 ± 0.01	1.43
IP-5	CH_3	C_6H_5	5.53 ± 0.28	4.68 ± 0.04	0.85
IP-7	C_6H_5	H	6.75 ± 0.22	4.68 ± 0.01	2.07
IP-9	C_6H_5	$CH_2C_6H_5$	5.89 ± 0.16	5.02 ± 0.01	0.87
IP-12	$CH_2C_6H_5$	H	6.12 ± 0.12	4.51 ± 0.01	1.61
IP-14	$(CH_2)_2C_6H_5$	H	7.50 ± 0.11	4.65 ± 0.01	2.85
IP-15	*t*-CH=CHC_6H_5	H	7.58 ± 0.06	5.82 ± 0.03	1.76
IP-17	*β*-naphthyl	H	8.20 ± 0.03	5.66 ± 0.02	2.54
IP-18	fur-2′-yl	H	5.57 ± 0.08	4.49 ± 0.05	1.08

[a] Standard errors for Supersomes calculated for the sigmoidal regression, not comparable with the standard deviation calculated on the average of different assays for rat enzyme. [b] ΔpIC$_{50}$: pIC$_{50}$ Supersomes − pIC$_{50}$ rat. [c] Highly significant ($P < 0.0001$, paired two-tailed student's t-test) difference of inhibition potency between human and rat MAO B.

Table 4. Supersomes and Rat Brain MAO B Inhibition Data for 5*H*-Indeno[1,2 -*c*]pyridazin-5-ones Derivatives (Series IV)

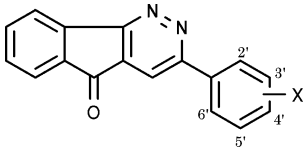

cmpd	X	pIC$_{50}$ Supersomes[a]	pIC$_{50}$ rat[a]	ΔpIC$_{50}$[b,c]
IP-7	H	6.75 ± 0.22	4.68 ± 0.04	2.07
IP-28	2′-CH_3	6.22 ± 0.10	4.51 ± 0.03	1.71
IP-31	4′-OH	6.57 ± 0.03	5.00 ± 0.07	1.57
IP-33	3′-OCH_3	7.37 ± 0.04	5.80 ± 0.05	1.57
IP-34	4′-OCH_3	7.13 ± 0.06	5.49 ± 0.01	1.64
IP-40	3′-F	7.37 ± 0.07	5.38 ± 0.02	2.00
IP-41	4′-F	7.83 ± 0.13	6.04 ± 0.03	1.79
IP-42	3′,4′-F_2	8.30 ± 0.12	6.04 ± 0.03	2.26
IP-43	2′-Cl	6.72 ± 0.12	4.80 ± 0.03	1.92
IP-44	3′-Cl	8.34 ± 0.15	6.05 ± 0.04	2.29
IP-45	4′-Cl	7.96 ± 0.16	6.04 ± 0.05	1.92
IP-47	3′-Br	8.25 ± 0.16	6.18 ± 0.03	2.07
IP-48	4′-Br	8.09 ± 0.04	5.88 ± 0.03	2.21
IP-50	3′-CF_3	8.07 ± 0.10	6.55 ± 0.03	1.52
IP-51	4′-CF_3	8.27 ± 0.13	7.05 ± 0.05	1.22
IP-53	3′-CN	7.48 ± 0.11	5.43 ± 0.04	2.05
IP-54	4′-CN	6.93 ± 0.25	5.66 ± 0.04	1.27
IP-55	2′-NO_2	6.28 ± 0.22	4.10 ± 0.02	2.18
IP-57	4′-NO_2	8.08 ± 0.05	6.30 ± 0.02	1.78
IP-59	4′-$COCH_3$	7.58 ± 0.05	5.75 ± 0.02	1.83
IP-62	4′-piperidyl	[d]	[d]	

[a] Standard errors for Supersomes calculated for the sigmoidal regression, not comparable with the standard deviation calculated on the average of different assays for rat enzyme. [b] ΔpIC$_{50}$: pIC$_{50}$ Supersomes − pIC$_{50}$ rat. [c] Highly significant ($P < 0.0001$, paired two-tailed student's t-test) difference of inhibition potency between human and rat MAO B. [d] No inhibition at maximum solubility.

series where variations are at positions 3 and 4 of the indenopyridazine ring (series III, Table 3, $n = 9$) and a series which contains 3-(substituted phenyl) indenopyridazines (series IV, Table 4, $n = 21$).

Comparison of in Vitro Inhibitor Potencies between Human and Rat MAO B. Comparison of pIC$_{50}$ values of coumarin and 5*H*-indeno[1,2-*c*]pyridazin-5-one derivatives determined with human and rat MAO B revealed important species-dependent differences in inhibitor selectivity between human and rat enzyme.

Figure 1 shows human pIC$_{50}$ values normalized with respect to the pIC$_{50}$ values of the most active human MAO B inhibitors (**C-19**, **C-57**) as a function of rat pIC$_{50}$ values normalized according to the pIC$_{50}$ values of the most active rat MAO B inhibitors (**C-61**, **C-64**). As can be noticed, no clear relationship exists between human and rat MAO B inhibition, neither considering all tested compounds together, nor taking into account each of the four series separately.

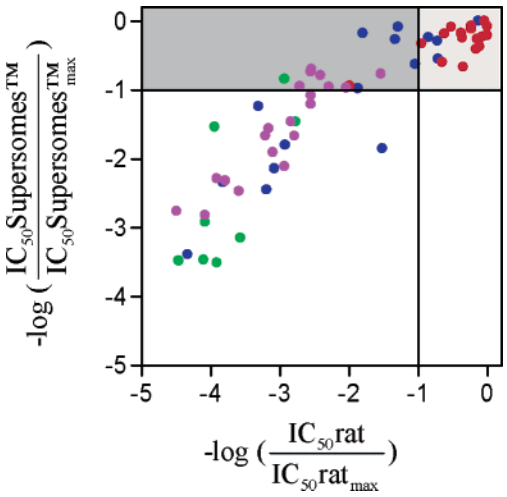

Figure 1. Human pIC$_{50}$ values normalized with respect to the pIC$_{50}$ value of the most active human MAO B inhibitors as a function of rat pIC$_{50}$ values normalized according to the pIC$_{50}$ value of the most active rat MAO B inhibitors: series I (blue solid dots), series II (red solid dots), series III (green solid dots) and series IV (purple solid dots). The gray areas qualify the prediction of human MAO B inhibitor potencies from rat MAO B pIC$_{50}$ values: compounds located in the light gray area are correctly predicted as interesting hits for the development of MAO B inhibitors; compounds located in the dark gray area are interesting hits missed by using the rat enzyme for hit selection.

Moreover, human MAO B inhibitor potencies are all higher than the ones toward rat brain MAO B obtained by Gnerre et al.[26] for coumarin derivatives and by Kneubühler et al.[27] for 5*H*-indeno[1,2-*c*]pyridazin-5-one derivatives, respectively. Indeed, the ΔpIC$_{50}$ values (difference between pIC$_{50}$ Supersomes and pIC$_{50}$ rat brain), were positive for all tested compounds (Tables 1, 2, 3, and 4). However, the extent of this difference varies largely between compounds, ranging from ΔpIC$_{50}$ values of 0.12 for compound **C-3** (Table 1) to ΔpIC$_{50}$ values of 2.85 for compound **IP-14** (Table 3). Hence, extrapolation from rat to human MAO B inhibitor potencies may result in a good estimation of human MAO B inhibitory activity, as in the case of compound **C-3**, but could also be off the mark by about 3 orders of magnitude, as for compound **IP-14**.

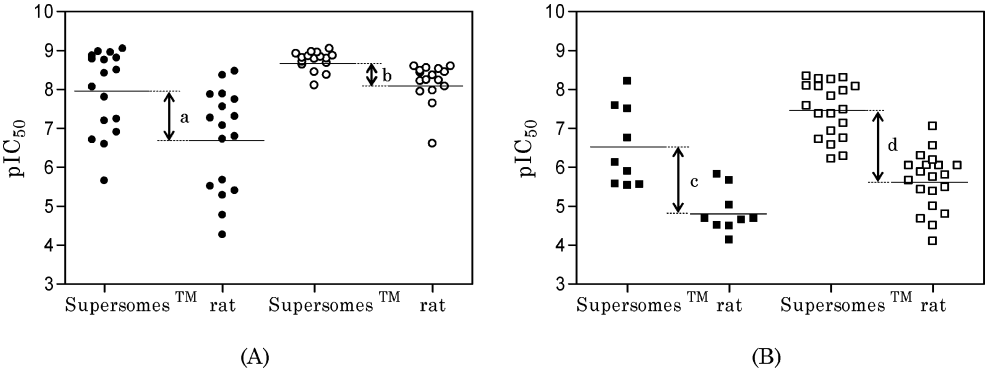

Figure 2. Dispersion of human and rat pIC_{50} values for series I (●) and series II (○) of coumarin derivatives (A) and for series III (■) and series IV (□) of 5*H*-indeno[1,2-*c*]pyridazin-5-one derivatives (B). Mean differences between human and rat MAO B inhibitor potencies (mean ΔpIC_{50}) are evidenced by double arrows indicated by different letters: (a) series I, (b) series II, (c) series III, and (d) series IV.

Additionally, as illustrated in Figure 2A for coumarin derivatives and in Figure 2B for 5*H*-indeno[1,2-*c*]pyridazin-5-one derivatives, the difference between human and rat MAO B inhibitor potencies is series-dependent. Indeed, for coumarin derivatives the mean ΔpIC_{50} values of the two series differ by almost 1 order of magnitude, the mean of ΔpIC_{50} being 1.25 (±0.31) for series I (evidenced by arrow a in Figure 2A) and 0.55 (±0.20) for series II (indicated by arrow b in Figure 2A), 95% confidence limits are given in parentheses. For the two series of 5*H*-indeno[1,2-*c*]pyridazin-5-one derivatives, the mean difference between human and animal enzyme is comparable (Figure 2B), the mean of ΔpIC_{50} being 1.67 (±0.55) for series III (evidenced by arrow c in Figure 2B) and 1.83 (±0.15) for series IV (indicated by arrow d in Figure 2B), 95% confidence limits are given in parentheses.

Interestingly, it can be noted that the difference between human and rat inhibitor potencies varies considerably among the two homogeneous series II and IV (mean ΔpIC50 value of 0.55 (±0.20) for series II vs 1.83 (±0.15) for series IV). Moreover, for human but not for rat MAO B, the dispersion of pIC_{50} values of the two series is significantly different (Fmax test), with series II presenting a narrower pIC_{50} scatter than series IV (Figure 2). Obviously, the influence of substituents on the in vitro inhibition of human MAO B differs markedly between these two homogeneous series.

Impact of Species-Dependent Differences on Hit Selection for the Development of MAO B Inhibitors. The divergences found between rodent and human MAO B inhibitory activities have important implications for the development of drugs involved in the MAO B metabolic pathway, suggesting that results obtained using rat tissues cannot be extrapolated to human CNS, a priori. In particular, these species-dependent differences may have a crucial impact on the identification of hit compounds for the development of new MAO B inhibitors. Indeed, it can be assumed that the selection of a hit compound for lead generation could not necessarily be the same using rat rather than human enzyme.

To evaluate the use of rat enzyme as a model to estimate human MAO B inhibitory potency, the plot of normalized human versus rat pIC_{50} values was taken into account (Figure 1). Inhibitors with pIC_{50} values within one unit from the most-active tested compound were considered as interesting hits for the development of MAO B inhibitors. Thus, compounds having inhibitor potencies of 1 order of magnitude from the most active inhibitor for both human and rat enzymes were retained for this evaluation, as delimited by black lines in Figure 1. The gray areas qualify the prediction of human MAO B inhibitor potencies from rat MAO B pIC_{50} values. Compounds located in the light gray area are correctly predicted as interesting hits for the development of MAO B inhibitors, whereas compounds located in the dark gray area are interesting hits missed by using the rat enzyme for hit selection.

Coumarin Derivatives of Series I. Based on rat MAO B inhibitor activities, Gnerre et al.[26] selected derivative **C-15** for hit refinement to generate series II and to explore SARs by various substitutions of the phenyl ring of the 7-benzyloxy group. Indeed, for rat MAO B inhibition, dimethyl substitution at positions 3 and 4 proved to be favorable, and **C-15** resulted in one of the most active inhibitors of series I toward rat enzyme.[26] In contrast, comparison between the human pIC_{50} value of the 3,4-dimethylated compound **C-15** and those of compounds unsubstituted at positions 3 and 4 (**C-2**), 4-methyl substituted (**C-10**), or bearing cycloaliphatic annelation at the 3- and 4-positions (**C-19**, **C-20**, **C-21**) showed that substitution at these positions has no remarkable influence on human MAO B inhibitor potency (Table 1). Moreover, a 7-benzylamino substituent (i.e., the presence of a $NHCH_2$ bridge at position 7) revealed to lower rat MAO B affinity, an effect that was not observable for human MAO B inhibition. Indeed, 7-benzylamino derivative **C-16** and 7-benzyloxy derivative **C-15** have comparable human pIC_{50} values (Table 1). Hence, although originally underestimated because of their low rat MAO B inhibitory activity, compounds **C-2**, **C-10**, **C-16**, **C-19**, **C-20**, and **C-21** appear to be interesting hits to generate leads for the development of human MAO B inhibitors.

Coumarin Derivatives of Series II. Concerning the inhibitory activities of 7-X-benzyloxy-substituted coumarin derivatives of series II, two principal observations can be made. All compounds of this series showed high activity toward both enzymes, except coumarin **C-56**, which appeared to be much less potent on rat MAO B (Table 2). Moreover, although the inhibitor potencies toward human and rat MAO B for this homogeneous series are significantly different, the species-dependent differences were markedly lower than those found for the other series tested. Therefore, for series II, rat inhibitor potencies can be considered as a good estimation of human MAO B inhibitory activities (Figure 1).

5*H*-Indeno[1,2-*c*]pyridazin-5-one Derivatives of Series III. The *trans*-styril (**IP-15**) and *β*-naphthyl (**IP-17**) derivatives are the most active compounds of series III toward human as well as rat MAO B. However, as a result of their poor solubility, neither of these compounds were selected by Kneubühler et al. for further optimization of rat brain MAO B inhibition. Promising preliminary results with *para*-substituted derivatives of compound **IP-7** motivated the choice of this compound to generate series IV.[27]

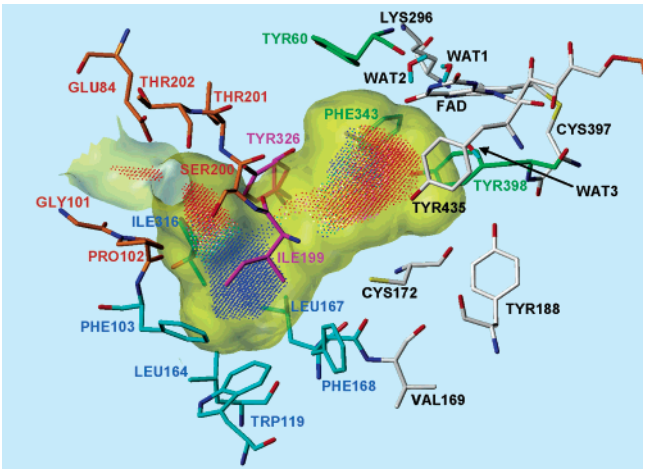

Figure 3. Binding site of MAO B, as used for molecular docking simulations. The Connolly channel surface of the cavities is displayed in translucent yellow. The colored dots describing the lipophilicity inside the pockets are color-coded according to their MLP values (see text). The amino acids potentially interacting with the ligands are color-coded following their localization around the binding site (see text). The flavine adenine dinucleotide cofactor (FAD) and the three selected water molecules (WATX) are represented as an integral part of the MAO B structure model.

The high human MAO B inhibitor potency of derivative **IP-14** indicates that this compound could also be selected to optimize the MAO B activity of this class of compounds. Indeed, the human MAO B inhibitory activity of **IP-14** is similar to the human MAO B inhibitor potency of **IP-15** and remarkably higher in comparison to its activity on rat enzyme ($\Delta pIC_{50} = 2.85$).

5*H*-Indeno[1,2-*c*]pyridazin-5-one Derivatives of Series IV. 5*H*-indeno[1,2-*c*]pyridazin-5-one derivatives of series IV are structurally homogeneous. Nevertheless, inhibitory activities of this series toward both enzymes vary markedly, as evidenced by the pIC_{50} values scatter plot (Figure 2B). This is in contrast to what was observed for the homogeneous coumarin series II. Moreover, for series IV, the mean difference in inhibitor potencies between human and rat enzyme is notably higher than that of coumarin series II. Thus, the poor correlation between human and rat MAO B inhibitory activity of series IV evidences notable species-dependent differences that make extrapolation from rat to human inhibition values difficult, even for these structurally homogeneous compounds.

Binding Mode Predictions by Molecular Docking into the Active Site of Human MAO B. To elucidate the different pIC_{50} scattering of coumarin series II and 5*H*-indeno[1,2-*c*]pyridazin-5-one series IV obtained in vitro with human recombinant enzyme, molecular docking of these homogeneous series within the active site of human MAO B was performed.

Description of the Binding Site of Human MAO B. The binding site region of the human MAO B crystallographic structure (PDB code 1oj9) after water molecule selection, molecular mechanics optimizations, and deletion of the cocrystallized ligand, as used for molecular docking simulations, is illustrated in Figure 3. It is shown that the three water molecules kept in the MAO B structure are all buried near the flavine adenine dinucleotide cofactor (FAD), this latter being covalently bound to CYS397. Two water molecules are involved in multiple H-bond networks (WAT1 and WAT2 in Figure 3), while the third one is fixed by the π-systems of the aromatic side chains of TYR398 and TYR435, as well as the central heterocyclic conjugated ring of FAD.

The Connolly channel surface in translucent yellow shows two distinct cavities inside the binding site. The first, so-called "entrance cavity", is connected to the outside of the protein, and the second, so-called "substrate cavity", is located in the vicinity of the FAD. These two cavities are separated by ILE199 and TYR326 (carbon atoms in violet in Figure 3) forming a bottleneck and thus acting as a gate, protecting the catalytic region from the outside. The side chain of ILE199 is the latch that separates the two cavities. It is displayed in Figure 3 as a rotamer in the "open" position, allowing the cocrystallized 1,4-diphenly-2-butene to reach both cavities.[29,30]

The dots inside the pockets, as described in the Experimental Section, are colored by the molecular lipophilicity potential (MLP) values using the following decreasing scales: polar values in red, magenta, orange, and yellow; hydrophobic values in blue, cyan, green-blue, and green.

It can be observed that the "substrate cavity" is mainly polar. This is explained by a number of polar side chains, accessible H-bonding groups, as well as the presence of the flavine nucleus and the three buried water molecules in the vicinity of this cavity. Only a pocket defined by three apolar residues, TYR60, PHE343, and TYR398 (carbon atoms in green in Figure 3), displays a hydrophobic environment.

In contrast to the polar property of the "substrate cavity", various zones displaying opposite lipophilicity are well-defined inside the "entrance cavity". The pocket coated by PHE103, TRP119, LEU164, LEU167, PHE168, and ILE316 displays a highly hydrophobic environment (carbon atoms in cyan in Figure 3), whereas another pocket toward the outside of the protein is surrounded by polar residues and amino acids with major H-bonding capacity (GLU84, GLY101, PRO102, SER200, THR201, THR202, and TYR326; carbon atoms in orange in Figure 3).

Evaluation of the Docking Procedure. Redocking of the cocrystallized ligand is a commonly used method to evaluate docking procedure efficiency. An extended conformation of 1,4-diphenyl-2-butene, obtained with the CONCORD algorithm and minimized with a standard BFGS procedure (see Experimental Section) was thus redocked into the binding site of the 1oj9 structure using three different strategies:

◦ Case A: Docking into the native protein, with no binding site optimization, no water molecules nor MLP fitting points filtering.

◦ Case B: Docking into the native protein without binding site optimization, but with three water molecules and MLP fitting points filtering.

◦ Case C: Docking into the optimized binding site, with three water molecules and MLP fitting points filtering (procedure described elsewhere,[31] see Experimental Section for details).

Calculation of RMSD values for each of the 20 docking solutions retrieved for each run referring to the native bound ligand showed clear advantage of keeping the three selected water molecules and using MLP filtering, as shown in Figure 4. Optimization of the binding site shows no significant improvement ($p = 0.056$, student's t-test) regarding RMSD values, as could be expected, because the side chain's relaxation does not modify thoroughly the global binding site topology (RMSD calculated between the native and the optimized side chains is 0.15 Å, whereas the backbone is not modified). Nevertheless, lower RMSD values are obtained in case C (minimal value = 0.98 Å) than in case B (minimal value = 1.11 Å). Moreover, the best-ranked docking solution in case C has a smaller RMSD value than its counterpart in case B.

Hence, our procedure consisting of docking into a preopti-

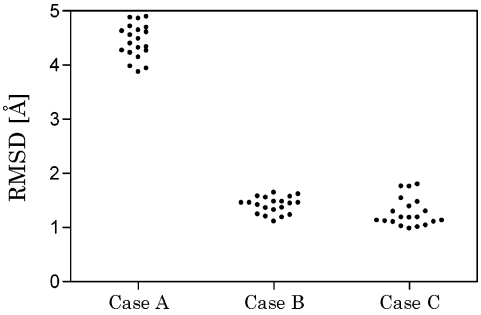

Figure 4. RMSD calculated between each docking solution and the reference cocrystallized pose in the 1oj9 complex (ligand = 1,4-diphenyl-2-butene). Case A: the ligand is docked into the native protein, without water molecules nor MLP fitting points filtering. Case B: the ligand is docked into the native protein without binding site optimization, but with three water molecules and MLP fitting points filtering. Case C: the ligand is docked into the optimized binding site, with water molecule selection and MLP fitting points filtering.

mized binding site, with water molecule selection and MLP fitting points filtering, appears reasonable and can be used for the docking of the coumarin and 5*H*-indeno[1,2-*c*]pyridazin-5-one derivatives.

Binding Mode Prediction of Coumarin Derivatives of Series II. The 16 3,4-dimethyl coumarins of series II, including various substitutions of the 7-benzyloxy group, are issued from compound **C-15**. As it could be expected, the docking solutions of this very homogeneous series are all superimposed to the binding mode of the unsubstituted coumarin **C-15**. All inhibitors of this series cross both cavities, presenting the coumarin nucleus inside the substrate cavity and the 7-X-benzyloxy group in a hydrophobic region of the entrance cavity (at the same place as the phenyl ring of cocrystallized 1,4-diphenyl-2-butene in 1oj9). For all docked 3,4-dimethyl-substituted coumarins, the rotation around the C7−O bond reflects the balance of the following intermolecular interactions:

◦ The position of the coumarin moiety is stabilized by H-bonds between the lactone oxygens, CYS172, TYR188, TYR435, and WAT3. The ether bridge is also potentially involved in a H-bond network, with different residues in the connecting zone between substrate and entrance cavities, notably with TYR326.

◦ The coumarin nucleus in the substrate cavity is placed to minimize unfavorable interactions between the methyl groups and the large polar region and/or to maximize hydrophobic interactions between the 4-methyl group and the small hydrophobic region (TYR60, PHE343, TYR398).

As described above, the entrance cavity is composed of two well-defined regions displaying opposite lipophilic properties, namely, a highly hydrophobic pocket and another pocket surrounded by polar residues and with major H-bond capacity amino acids. Therefore, all kinds of substituents of the 7-benzyloxy ring are able to find favorable interactions to stabilize the complex in the entrance cavity. This is illustrated in Figure 5, where polar substituents such as acetamide (**C-56**) are placed in the polar pocket, while hydrophobic moieties such as methyl (**C-51**) or chlorine (**C-64**) find a favorable environment in the hydrophobic pocket.

Binding Mode Prediction of 5*H*-Indeno[1,2-*c*]pyridazin-5-one Derivatives of Series IV. Series IV contains 5*H*-indeno-[1,2-*c*]pyridazin-5-one derivatives that are issued from compound **IP-7** by various substitutions at the 3-phenyl ring.[27] Docking solutions of these 20 derivatives are all similar to the binding mode of the lead inhibitor **IP-7** and well superposed on it. The 3-phenyl moiety is in the substrate cavity that appears

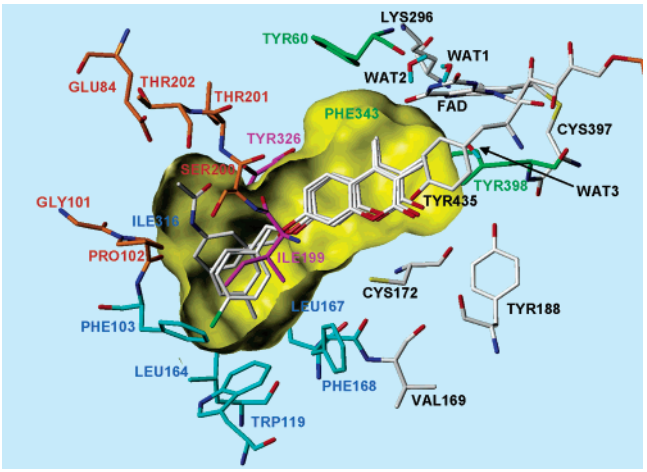

Figure 5. Docking solutions of representative coumarin derivatives belonging to series II (**C-51**, **C-56**, and **C-64**). The Connolly channel surface of the cavities is displayed in opaque yellow. The residues potentially interacting with the ligands are represented and colored following the topological rules described in Description of the Binding Site (see Figure 3).

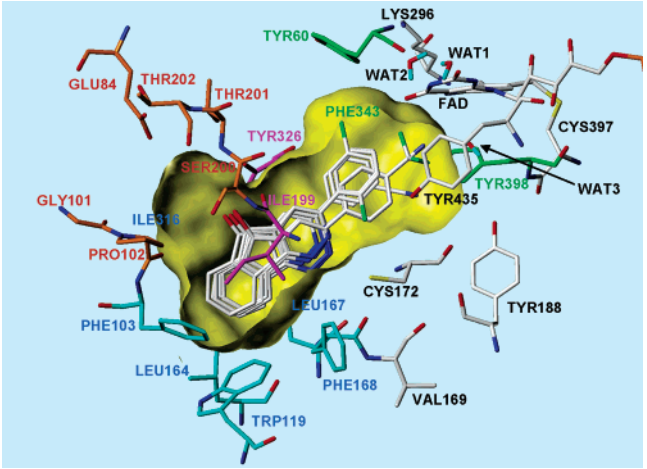

Figure 6. Docking solutions of representative 5*H*-indeno[1,2-*c*]-pyridazin-5-one derivatives belonging to series IV (**IP-28**, **IP-43**, **IP-44**, **IP-47**, **IP-51**, **IP-53**, **IP-54**, and **IP-55**). The Connolly channel surface of the cavities is displayed in opaque yellow. The residues potentially interacting with the ligands are represented and colored following the topological rules described in Description of the Binding Site (see Figure 3).

to be able to accommodate all studied substituents following minor positioning adjustments. However, the substrate cavity being more sterically constrained than the entrance cavity and characterized by a large polar region and a small hydrophobic zone, 5*H*-indeno[1,2-*c*]pyridazin-5-one derivatives of series IV are forced to find interactions between the substituted phenyl groups and the residues coating the substrate cavity that are not necessarily favorable. This can explain why some of these compounds exhibit modest human inhibitory activities. As shown in Figure 6, this is the case for compounds substituted at position 2′ of the phenyl ring (**IP-28**, **IP-43**, **IP-55**) and others bearing cyano substitution of the phenyl ring at position 3′ or 4′ (**IP-53**, **IP-54**). In contrast, compounds bearing hydrophobic substitution at position 3′ (**IP-44**, **IP-47**, **IP-51**) are among the most active inhibitors of the series, in agreement with their ability to reach the hydrophobic pocket (TYR60, PHE343, TYR398), finding a favorable environment.

Interpretation of the Difference in Substituent Effects on Human MAO B Inhibitor Potencies between Series II and

IV. Docking solutions within human MAO B for coumarin series II and 5*H*-indeno[1,2-*c*]pyridazin-5-one series IV have evidenced different binding modes, allowing to clarify the different pIC_{50} scattering of the two homogeneous series.

Homogeneous superposed docking solutions of series II within the human enzyme show that the coumarin nucleus is located in the substrate cavity near the FAD cofactor (Figure 5). Thus, the various substitutions of the phenyl ring of the 7-benzyloxy group do not show a remarkable influence on the inhibitor potency, all substituents being well-accommodated by the entrance cavity.

On the other hand, the opposite is observed for series IV. Indeed, the binding modes of these compounds exhibit the 5*H*-indeno[1,2-*c*]pyridazin-5-one nucleus in the entrance cavity, while the 3-X-phenyl ring is located in the substrate cavity near the FAD cofactor (Figure 6). Hence, the nature of the different substituents of the phenyl ring influences markedly binding and, thus, activity toward human MAO B.

Hypothesis about Structural Variations between Human and Rat MAO B Binding Sites. In vitro results showed that the difference between human and rat inhibitor potencies is notably lower for series II than for series IV (mean ΔpIC_{50} value 0.55 ($\pm$0.20) for series II vs 1.83 ($\pm$0.15) for series IV). The lager species-dependent differences found for series IV, having the differently substituted 3-X-phenyl ring located in the substrate cavity near the FAD cofactor, could be attributed to structural variations of this cavity between human and rat enzymes. Because human and rat MAO B have an 88% sequence identity and a 93% sequence homology,[25] these structural variations might be relevant in the secondary or tertiary structures. Only a crystallographic analysis of the rat MAO B enzyme and subsequent molecular docking simulations would validate this hypothesis without doubt.

Conclusions

Important species-dependent differences in MAO B inhibitor specificity between human and rat have been evidenced for two classes of compounds. Both coumarin and 5*H*-indeno[1,2-*c*]-pyridazin-5-one derivatives have shown a greater inhibitor potency toward human enzyme than toward rat MAO B. Moreover, no clear correlations were found between the inhibition of the two enzymes for these two classes of compounds. These differences in MAO B inhibitor specificity revealed to be series-dependent.

Because rodents are a very common source of MAO B for inhibitor screening, the species-dependent differences evidenced in the present work are of critical importance and could influence the identification of hit compounds for the design and development of new MAO B inhibitors. It can be assumed that the choice of a hit compound for hit refinement and lead generation could not necessarily be the same using human rather than rat enzyme. Among the four series investigated, only pIC_{50} values of coumarin series II were similar enough between the two species to allow prediction of human MAO B inhibitory activities from rat inhibitor potencies.

The different inhibition patterns of the two homogeneous series II and IV obtained in vitro with human recombinant MAO B, can be explained by their different binding modes. Docking solutions into the active site of human MAO B for series II and IV have clearly evidenced different binding modes for the two series. Indeed, for 5*H*-indeno[1,2-*c*]pyridazin-5-one derivatives of series IV, the nature of the different substituents of the phenyl ring influences markedly binding and thus activity toward human MAO B, the various substituents of the phenyl ring being located in the substrate cavity near the FAD cofactor. The opposite is observed for coumarin derivatives of series II, all substituents of the phenyl ring of the 7-benzyloxy group being well-accommodated by the entrance cavity.

Experimental Section

Materials. Kynuramine was obtained from Sigma-Aldrich Chemical (St. Louis, MA). DMSO (microselect for molecular biology), 4-hydroxyquinoline, potassium phosphate salts, potassium chloride, and sodium hydroxide came from Fluka AG (Buchs, CH). The synthesis of all compounds not commercially available was performed in the Dipartimento Farmaco-Chimico, Università di Bari, I-70125, Bari, Italy. The details of the synthesis of coumarin derivatives (**C**) have been reported by Gnerre et al.,[26] except for compound **C-75**, which was synthesized later and described by Novaroli et al.[28]

The synthesis of 5*H*-indeno[1,2-*c*]pyridazin-5-one derivatives (**IP**) has been described by Carotti et al.[32] for compounds **IP-14**, **17**, **31**, **53**, and **55**, and by Kneubühler et al. for compounds **IP-4**, **7**, **9**, **12**, **15**, **18**, **28**, **34**, **41**, **43**, **44**, **45**, **47**, **50**, and **57** in reference 33, and for compounds **IP-33**, **40**, **42**, **48**, **51**, **54**, **59**, and **62** in reference 27.

Biological Assays. Supersomes. Human MAO B Supersomes, purchased from BD Gentest (Woburn, MA), are mitochondrial membrane fractions containing human recombinant MAO B. Supersomes were stored at −80 °C. After initial thawing, small aliquots were refrozen to avoid multiple freezing and thawing sequences.

MAO B inhibition assays were carried out with a fluorescence-based method (end-point lecture) using kynuramine as substrate. The detailed description of the method has been reported previously.[28] Briefly, reactions were performed in black, flat-bottomed polystyrene 96-well microtiter plates (FluoroNunc/LumiNunc, MaxiSorpTM surface, NUNC, Roskild, Denmark) containing potassium phosphate buffer, an aqueous stock solution of kynuramine, and DMSO inhibitor solution. This assay mixture was preincubated at 37 °C, and then the diluted human recombinant enzyme was delivered to obtain a final protein concentration of 0.015 mg/mL. Incubation was carried out at 37 °C, and the reaction was stopped by addition of NaOH.

Formation of 4-hydroxyquinoline was quantified with a 96-well microplate fluorescent reader (FLx 800, Bio-Tek Instruments, Inc., Winooski, U.S.A.) at excitation/emission wavelengths of 310/400 nm (20 nm slit width for excitation, 30 nm slit width for emission).

Data analysis was performed with Prism V4.0 (GraphPad Software. Inc.). The degree of inhibition pIC_{50} ($-\log IC_{50}$) was assessed by a sigmoidal dose−response curve.

Molecular Docking Simulations. MAO B Crystal Structure. Among the various crystallographic structures of human MAO B available, the 1oj9 complex was retrieved from the Brookhaven Protein Database (PDB; http://www.rcsb.org/pdb/)[34] for docking simulations. This choice was guided by the quality of the crystallographic data and the fact that 1,4-diphenyl-2-butene was (at the time of the simulation) the only cocrystallized noncovalent ligand crossing the entire binding site of MAO B. As a consequence, the side chain of key residue ILE199 is oriented such as the "entrance" and "substrate" cavities are fused (see Description of the Binding Site in Results). This structural prerogative is essential to model the binding of coumarin and 5*H*-indeno[1,2-*c*]pyridazin-5-one derivatives that must be accommodated by both cavities.[29,35]

Alignment of several other crystallographic structures of human MAO B allowed to identify and select three conserved water molecules buried in the vicinity of FAD (see Description of the Binding Site in Results). These well-described fixed water molecules[35] are kept inside the 1oj9 binding site as an integral part of the protein structure during the whole computational procedure because retaining them was demonstrated to be beneficial for docking and virtual screening simulations toward MAO B.[36]

Hydrogen atoms were added to 1oj9 containing the three water molecules in agreement with the ionization state existing at

physiological pH. Partial atomic charges were computed according to the Gasteiger−Marsili method.[37] Aggregate was defined as backbone, oxygen of the water molecules, and all substructures outside a sphere of 8 Å around 1,4-diphenyl-2-butene. This structure was then submitted to a simulated annealing procedure within a modified Tripos force field[38] consisting in stabilization at 500 K during 2000 fs and cooling exponentially to 150 K in 1000 fs. The resulting geometry after five cycles was subsequently minimized by a standard BFGS procedure of a maximum of 6000 steps based on a modified Tripos force field.

The user-defined binding site was simplified as a sphere. Its center was fixed as the coordinates of 1,4-diphenyl-2-butene centroid, using all heavy atoms, and its radius was set to 15 Å. Subsequently, 1,4-diphenyl-2-butene and crystallization artifacts were removed.

Ligand Modeling. The starting geometries of the coumarin and 5*H*-indeno[1,2-*c*]pyridazin-5-one derivatives to be docked were built using the CONCORD algorithm,[39] and the ionization state was defined as appropriate at pH 7.4. They were optimized by a standard BFGS minimization procedure of a maximum of 6000 steps based on a modified Tripos force field including Gasteiger−Marsili partial atomic charges.

Docking Procedure. Automated docking was carried out using the program GOLD (Genetic Optimization for Ligand Docking) version 2.2.[40,41] This docking engine is a widely employed genetic algorithm-based commercial software that considers total ligand flexibility. Moreover, it permits some protein conformational freedom in the sense that torsion angles of serine, threonine, and tyrosine hydroxyl groups as well as lysine amine groups are optimized by the search algorithm during the posing. These groups are allowed to rotate freely to favor intramolecular (with other residues of the protein) and intermolecular (with the ligand trial solution) H-bond formation. The embedded GoldScore function,[42] used for scoring to evaluate docking solutions, is based on a simplified force field for steric interactions (Lennard−Jones potential) and electrostatic terms (Coulombic potential). Moreover, hydrogen bonds are taken into account explicitly depending on the nature and geometry of the given interaction. Furthermore, a torsional entropy term for ligands is included in GoldScore to account for the loss of entropy when a bond is kept rigid.

In its first stage, GOLD generates *hydrophobic fitting points* in the binding site to guide the placement of hydrophobic ligand atoms.[43] To better characterize hydrophobicity, the molecular lipophilicity potential (MLP) based on *n*-octanol/water partition coefficients was used.[44] The MLP was calculated on every point defined by GOLD as hydrophobic, and only the dots bearing positive MLP values were kept as final hydrophobic fitting points. This "MLP-filter" was used here in all simulations, since it was established to improve docking of ligands using GOLD and especially docking of MAO B inhibitors. The theoretical and methodological aspects are explained in details elsewhere.[36] The resulting graphical description of the lipophilicity inside MAO B cavities appears in "Description of the Binding Site of MAO B" (see Figure 3) in Results.

No constraint was given and default parameters were set for the genetic algorithm used by GOLD to explore possible poses and for the GoldScore function to evaluate binding. For each ligand, 20 solutions were allowed. The representative poses retained to define the binding modes correspond to the highest scored solution for each inhibitor.

References

(1) Foley, P.; Gerlach, M.; Yuodim, M. B. H.; Riederer, P. MAO-B inhibitors: multiple roles in the therapy of neurodegenerative disorders? *Parkinsonism Relat. Disorders* **2000**, *6*, 25−47.

(2) Nicotra, A.; Pierucci, F.; Parvez, H.; Senatori, O. Monoamine oxidase expression during development and aging. *Neurotoxicology* **2004**, *25*, 155−165.

(3) Delumeau, J. C.; Bentué-Ferrer, D.; Gandon, J. M.; Amrein, R.; Belliard, S.; Allain, H. Monoamine oxidase inhibitors, cognitive functions and neurodegenerative diseases. *J. Neural Transm.* **1994**, *41*, 259−266.

(4) Strolin Benedetti, M.; Dostert, P. Monoamine oxidase, brain aging and degenerative diseases. *Biochem. Pharmacol.* **1989**, *38*, 555−561.

(5) Shih, J. C.; Chen, K.; Ridd, M. J. Monoamine oxidase: from genes to behavior. *Annu. Rev. Neurosci.* **1999**, *22*, 197−217.

(6) Mellick, G. D.; Buchanan, D. D.; McCann, S. J.; James, K. M.; Johnson, A. G.; Davis, D. R.; Liyou, N.; Chan, D.; LeCouteur, D. G. Variations in the monoamine oxidase B (MAOB) gene are associated with Parkinson's disease. *Movement Disorders* **1999**, *14*, 219−224.

(7) Barnham, K. J.; Masters, C. L.; Bush, A. I. Neurodegenerative diseases and oxidative stress. *Nat. Rev.* **2004**, *3*, 205−214.

(8) Youdim, M. B. H.; Fridkin, M.; Zheng, H. Novel bifunctional drugs targeting monoamine oxidase inhibition and iron chelation as an approach to neuroprotection in Parkinson's disease and other neurodegenerative diseases. *J. Neural Transm.* **2004**, *111*, 1455−1471.

(9) Yamada, M.; Yasuhara, H. Clinical pharmacology of MAO inhibitors: safety and future. *Neurotoxicology* **2004**, *25*, 215−221.

(10) Palhagen, S.; Heinonen, E.; Hägglund, J.; Kaugesaar, T.; Mäki-Ikola, O.; Palm, R. Selegiline slows the progression of the symptoms of Parkinson disease. *Neurology* **2006**, *66*, 1200−1206.

(11) Naoi, M.; Hirata, Y.; Nagatsu, T. Inhibition of monoamine oxidase by *N*-methylisoquinolinium ion. *J. Neurochem.* **1987**, *48*, 709−712.

(12) Bembenek, M. E.; Abell, C. W.; Chrisey, L. A.; Rozwadowska, M. D.; Gessner, W.; Brossi, A. Inhibition of monoamine oxidases A and B by simple isoquinoline alkaloids: racemic and optically active 1,2,3,4-tetrahydro-3,4-dihydro- and fully aromatic isoquinolines. *J. Med. Chem.* **1990**, *33*, 147−152.

(13) Donnelly, C. H.; Murphy, D. L. Substrate- and inhibitor-related characteristics of human platelet monoamine oxidase. *Biochem. Pharmacol.* **1977**, *26*, 852−858.

(14) Wirz-Justice, A. Platelet research in psychiatry. *Experientia, Suppl.* **1988**, *44*, 145−152.

(15) Mazouz, F.; Gueddari, S.; Burstein, C.; Mansuy, D.; Milcent, R. 5-[4-(Benzyloxy)phenyl]-1,3,4-oxadiazol-2(3H)-one derivatives and related analogues: new reversible, highly potent, and selective monoamine oxidase type B inhibitors. *J. Med. Chem.* **1993**, *36*, 1157−1167.

(16) Chiba, K.; Trevor, A.; Castagnoli, N. Metabolism of the neurotoxic tertiary amine, MPTP, by brain monoamine oxidase. *Biochem. Biophys. Res. Commun.* **1984**, *120*, 574−578.

(17) Snyder, S. H.; Hendley, E. D. A simple sensitive fluorescence assay for monoamine oxidase and diamine oxidase. *J. Pharmacol. Exp. Ther.* **1968**, *163*, 368−392.

(18) Mazouz, F.; Lebreton, L.; Milcent, R.; Burstein, C. 5-Aryl-1,3,4-oxadiazol-2(3H)-one derivatives and sulfur analogues as new selective and competitive monoamine oxidase type B inhibitors. *Eur. J. Med. Chem.* **1990**, *25*, 659−671.

(19) Yu, P. H. Deamination of aliphatic amines of different chain lengths by rat liver monoamine oxidase A and B. *J. Pharm. Pharmacol.* **1989**, *41*, 205−208.

(20) Ali, A.; Robinson, J. B. Synthesis, biological evaluation and quantitative structure activity relationship analysis of nuclear-substituted pargylines as competitive inhibitors of MAO-A and MAO-B. *J. Pharm. Pharmacol.* **1991**, *43*, 750−757.

(21) O'Brien, E. M.; Dostert, P.; Tipton, K. F. Species differences in the interactions of the anticonvulsant milacemide and some analogues with monoamine oxidase-B. *Biochem. Pharmacol.* **1995**, *50*, 317−324.

(22) Reid, A. A.; Hill, J. L.; Murphy, D. L. Interactions of tricyclic antidepressant drugs with human and rat monoamine oxidase type B. *Naunyn-Schmiedeberg's Arch. Pharmacol.* **1988**, *338*, 678−683.

(23) Denney, R. M.; Patel, N. T.; Fritz, R. R.; Abell, C. W. A monoclonal and specificity for human monoamine oxidase B but not A. *Mol. Pharmacol.* **1982**, *22*, 500−508.

(24) Denney, R. M.; Denney, C. B. An update on the identity crisis of monoamine oxidase: new and old evidence for the independence of MAO A and B. *Pharmacol. Ther.* **1985**, *30*, 227−259.

(25) Geha, R. M.; Chen, K.; Shih, J. C. Phe^{208} and Ile^{199} in human monoamine oxidase A and B do not determine substrate and inhibitor specificities as in rat. *J. Neurochem.* **2000**, *75*, 1304−1309.

(26) Gnerre, C.; Catto, M.; Leonetti, F.; Weber, P.; Carrupt, P. A.; Altomare, C.; Carotti, A.; Testa, B. Inhibition of monoamine oxidases by functionalized coumarin derivatives: biological activities, QSARs, and 3D-QSARs. *J. Med. Chem.* **2000**, *43*, 4747−4758.

(27) Kneubühler, S.; Thull, U.; Altomare, C.; Carta, V.; Gaillard, P.; Carrupt, P. A.; Carotti, A.; Testa, B. Inhibition of monoamine oxidase-B by 5*H*-indeno[1,2-*c*]pyridazine derivatives: biological activities, quantitative structure−activity relationships (QSARs) and 3D-QSARs. *J. Med. Chem.* **1995**, *38*, 3874−3883.

(28) Novaroli, L.; Reist, M.; Favre, E.; Carotti, A.; Catto, M.; Carrupt, P. A. Human recombinant monoamine oxidase B as reliable and efficient enzyme source for inhibitor screening. *Bioorg. Med. Chem.* **2005**, *13*, 6212−6217.
(29) Binda, C.; Newton-Vinson, P.; Hubälek, F.; Edmondson, D. E.; Mattevi, A. Structure of human monoamine oxidase B, a drug target for the treatment of neurological disorders. *Nat. Struct. Biol.* **2001**, *10*, 1−5.
(30) Veselovsky, A. V.; Ivanov, A. S.; Medvedev, A. E. Computer modelling and visualization of active site of monoamine oxidases. *Neurotoxicology* **2004**, *25*, 37−46.
(31) Daina, A.; Rey, S.; Novaroli, L.; Reist, M.; Carrupt, P. A. Pre- and postprocessing molecular interaction fields tools in receptor-based drug design strategy towards neurodegenerative diseases. *Chimia* **2005**, *59*, 603.
(32) Carotti, A.; Carta, V.; Campagna, F.; Altomare, C.; Casini, G. An efficient route to biologically active 5*H*-indeno[1,2-*c*]-pyridazin-5-ones. *Farmaco* **1993**, *48*, 137−141.
(33) Kneubühler, S.; Carta, V.; Altomare, C.; Carotti, A.; Testa, B. Synthesis and monoamine oxidase activity of 3-substituted 5*H*-indeno[1,2-*c*]pyridazines. *Helv. Chim. Acta* **1993**, *76*, 1954−1963.
(34) Berman, H. M.; Westbrook, J.; Feng, Z.; Gilliland, G.; Bhat, T. N.; Weissig, H.; Shindyalov, I. N.; Bourne, P. E. The protein data bank. *Nucleic Acids Res.* **2000**, *28*, 235−242.
(35) Binda, C.; Li, M.; Hubälek, F.; Restelli, N.; Edmondson, D. E.; Mattevi, A. Insights into the mode of inhibition of human mitochondrial monoamine oxidase B from high-resolution crystal structures. *Proc. Natl. Acad. Sci. U.S.A.* **2003**, *100*, 9750−9755.
(36) Daina, A.; Rey, S.; Ooms, F.; Bravo, J.; Boccard, J.; Carrupt, P. A. Toward a better description of hydrophobicity using the Molecular Lipophilicity Potential (MLP) within a GOLD docking strategy. To be submitted for publication, 2006.
(37) Gasteiger, J.; Marsili, M. Iterative partial equalization of orbital electronegativity: a rapid access to atomic charges. *Tetrahedron* **1980**, *36*, 3219−3222.
(38) Clark, M.; Cramer, R. D., III; Van Opdenbosch, N. Validation of the general purpose Tripos 5.2 force field. *J. Comput. Chem.* **1989**, *10*, 982−1012.
(39) Pearlman, R. S.; Balducci, R.; Rusinko, A.; Skell, J. M.; Smith, K. M. *CONCORD 3.0.1.*; Tripos Associates, Inc.: St. Louis, Missouri, 1993.
(40) Nissink, J. W.; Murray, C.; Hartshorn, M.; Verdonk, M. L.; Cole, J. C.; Taylor, R. A new test set for validating predictions of protein−ligand interactions. *Proteins: Struct., Funct., Genet.* **2002**, *49*, 457−471.
(41) *SYBYL 7.0.*; Tripos Associates, Inc.: St. Louis, Missouri, 2004.
(42) Verdonk, M. L.; Cole, J. C.; Hartshorn, M. J.; Murray, C. W.; Taylor, R. D. Improved protein−ligand docking using GOLD. *Proteins: Struct., Funct., Genet.* **2003**, *52*, 609−623.
(43) *GOLD*, version 2.0; Online Documentation (http://www.ccdc.co.uk); Cambridge Crystallographic Data Center: Cambridge, U.K., 2002.
(44) Gaillard, P.; Carrupt, P. A.; Testa, B.; Boudon, A. Molecular lipophilicity potential, a tool in 3D-QSAR. Method and applications. *J. Comput.-Aided Mol. Des.* **1994**, *8*, 83−96.

JM060441E